Bi-monthly • July - August • 2020 • Issue No. 369 ISSN: 0976-2108

BARC NEWSLETTER

UV Illuminated Plastic Detector

This page is intentionally left blank

CONTENTS

This page is intentionally left blank

Technology for preparation of low-carbon ferrochromium from Indian chrome ore by aluminothermy process

Sanjib Majumdar*, Bhaskar Paul, Jugal Kishor, Vivekanand Kain
Materials Processing and Corrosion Engineering Division, BARC

Abstract

Using Indian chrome ore as the starting material, ferrochromium alloy containing very low carbon (~0.02%), aluminium (0-0.5%), and other impurities has been prepared, and the associated technology was successfully demonstrated. High quality ferrochromium is the key ingredient for producing special grades of steels having improved characteristics such as increased resistance to corrosion, high-temperature oxidation and enhanced mechanical properties. The process parameters of aluminothermic coreduction technique were carefully optimized to prepare high quality ferrochromium alloy comprising Fe-60 wt % Cr. Important constituents of the thermit charge, including Indian chrome ore, hematite, heat booster, reducing agent (Al), and other additives were tried in varied proportions across numerous experiments to achieve a maximum thermit yield of 72.5% with a 70% recovery in Cr metal. Thermodynamic parameters of the reduction reactions were optimized for achieving good slag/metal separation, and high purity thermit ferrochromium product.

Keywords: Coreduction, Thermit process, Enthalpy, Ferrochromium, Aluminium

Introduction

Special quality ferroalloys are necessary for production of high-grade alloy steels. Low-carbon and low-aluminium containing ferrochromium is one of the most important ferroalloys used in the production of special grades of steels having superior corrosion and high-temperature oxidation resistance properties. The preparation of low-carbon ferrochromium using chrome ore was first carried out at a furnace in Russia's Chelyabinsk Electrometallurgical Combine plant in the year 1976 [1]. The influence of the phosphorus content of the charge materials on the concentration of P in low-carbon ferrochromium produced by mixing an ore-lime melt with liquid silicochrome was investigated earlier [2]. High-carbon ferrochromium is most extensively used for production of chromium steels, mainly stainless steels [3]. The high carbon ferrochromium is produced in the electric arc furnace by using carbon as a reducing agent. However, a number of refining steps are required in oxygen-intensive steel making process to reduce the carbon content in the steel. Silicothermy process is used most widely for production of low-carbon ferrochromium [4]. However, the product alloy contains a significant amount of silicon. Therefore, the preparation of ferrochromium containing low amount of the reducing elements used (e.g. C, Si, Al) is a challenging task. In the present work, aluminothermic coreduction process was demonstrated for preparation of low-carbon and low-aluminium containing ferrochromium using Indian chrome ore. The charge composition was optimized to achieve higher yield of the thermit product. The product was characterized using scanning electron microscopy and energy dispersive spectrometry.

Equipment and Method

Fig. 1 represents the schematic diagram of the specially-designed thermit reactor for carrying out aluminothermy process. The thermit reactor is a steel vessel with the inner lining made up of refractory material. The reactor is placed on a metallic tray containing a layer of refractory powder. The entire assembly is dried or pre-heated to about 150°C before its use. The composition of Indian chrome ore is presented in Table 1. The major constituents of the ore are Cr_2O_3 (59% by wt.), Fe_2O_3 (19%), MgO (11%) and Al_2O_3 (10%). While MgO and Al_2O_3 join the slag phase, the coreduction of Cr_2O_3 and Fe_2O_3 is carried out using the reducing agent aluminium (Al) during the thermit process. The ferrochromium composition targeted in this work was Fe-60 wt.% Cr. For achieving this composition, Fe_2O_3 powder was used as an additive. Industrially, mill scales are used in spite of pure hematite; however, the composition of the mill scale should be confirmed before its use. The other additives used for carrying out the thermit process are heat booster, slag fluidiser etc. Sodium nitrate ($NaNO_3$) was used as a heat booster for the present work. Other additives used are CaO, CaF_2 etc. The typical composition of the charge of the aluminothermy process is presented in Table 2.

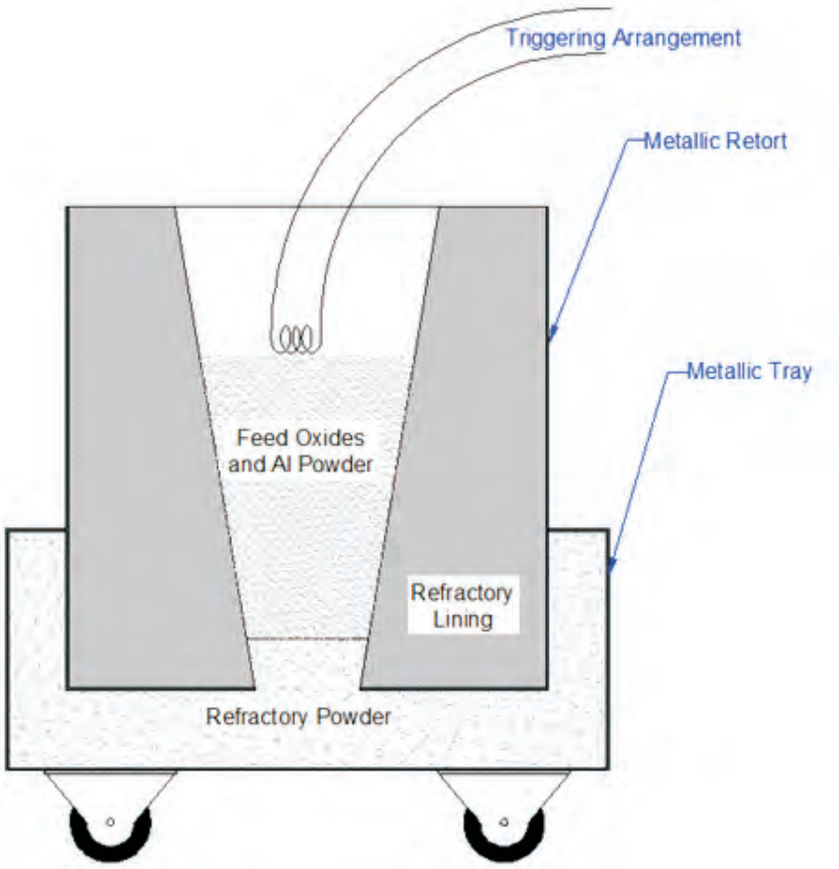

Fig. 1: Schematic diagram of the reactor assembly used for aluminothermy process

Table 1: Chemical analysis (in wt.%) of the Indian Chrome ore

Cr_2O_3	SiO_2	Fe_2O_3	Al_2O_3	CaO	MgO	P	S
59.16	1.16	19.0	9.75	0.286	10.63	0.008	0.006

The chrome ore, hematite and other oxide additives are pre-heated separately in the temperature ranging from 400 to 900°C. After cooling, the desired quantities of the individual powder are weighed, and mixed intimately along with aluminium and $NaNO_3$ powder using a tumbler mixer. The particle size of the powder plays a very important role on the final yield of the process. The mixed charge (powder) is subsequently placed inside the thermit reactor as shown in Fig. 1. The reduction reaction is initiated or triggered by bringing into contact the top surface of the charge with a burning magnesium ribbon or a resistance-heated coil. Following which, the reaction proceeds autogenously and gets completed within 1-5 minutes depending upon the amount of the charge used. A number of such experiments were carried out using different compositions of charge ranging from 100g to 1000g. After cooling the reactor, the metallic portion of the thermit product is separated from the slag. The thermit product/button is weighed to understand the product yield. Subsequently, the thermit ferrochromium button is broken into small chunks using a jaw crusher. Characterization and analysis of the

Table 2: Results obtained from different thermit experiments for a targeted ferrochromium composition of Fe-60Cr (wt.%)

Expt. No.	Aluminothermy charge composition (in g)					Thermit product yield (in %)	Analysis of the thermit product (Fr -Cr), in wt.%			
	Indian Chrome ore	Fe_2O_3	Al (Reducing agent)	$NaNO_3$ (Heat booster)	CaO		Cr	Fe	Al	Si
1	100	19.3	39	9	-	62.5	57	37	5	1
2	100	20	38.7	12	10	51	53. 5	38	7	1.5
3	100	17.4	36	12	-	68.7	55. 3	40. 8	3	0.9
4	100	20	36	10	-	72.5	59. 5	40. 5	-	-

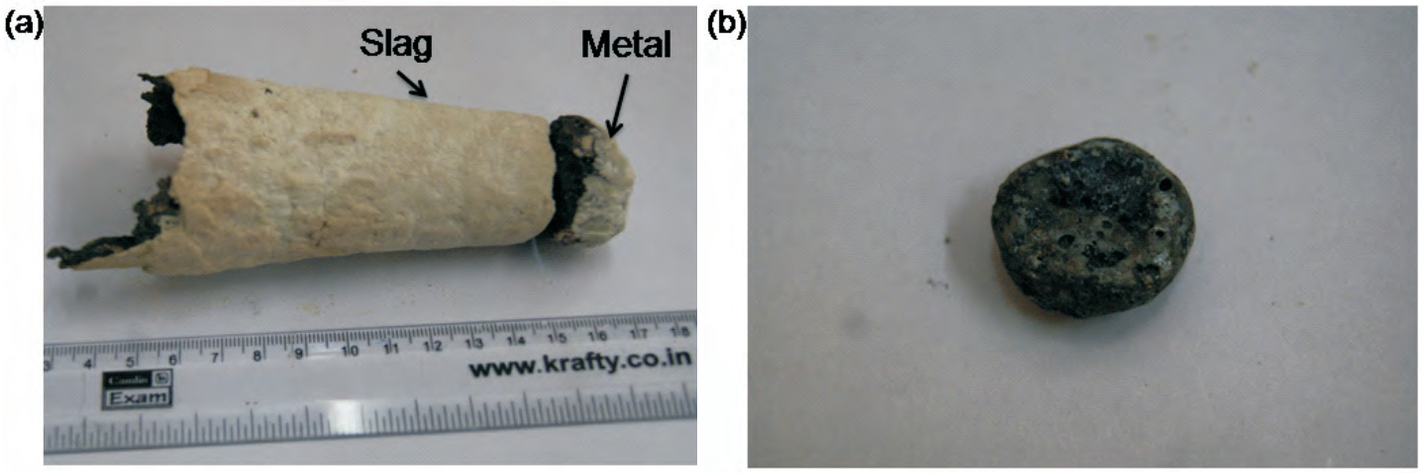

Fig. 2: Outlook of the thermit products; (a) both slag and metal parts are present, and (b) the metallic ferrochromium product

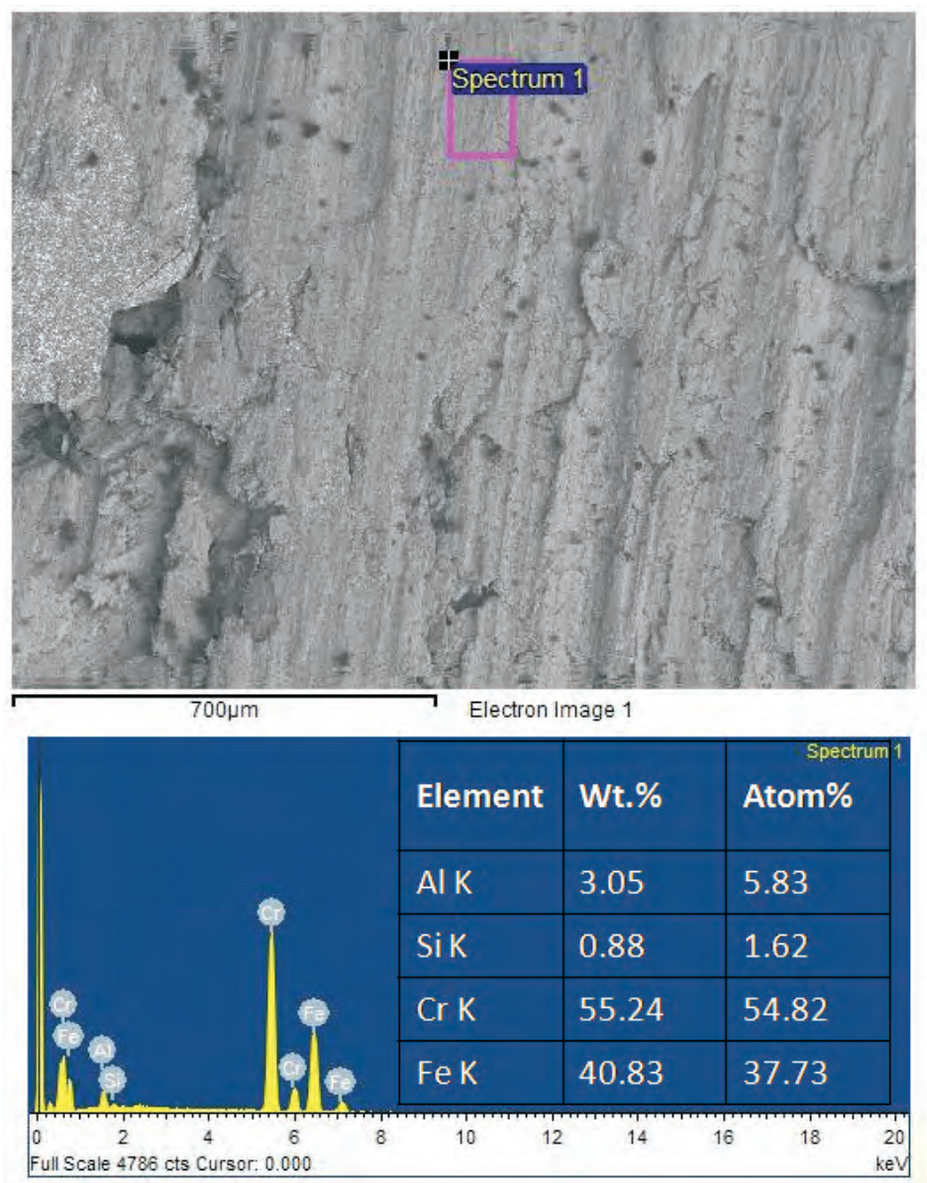

Fig. 3: SEM image, and EDS analysis of the ferrochromium obtained from experiment no. 3 in Table 2

ferrochromium product was carried out using scanning electron microscopy (SEM) and energy dispersive spectrometry (EDS).

Results and Discussion

(a) Thermit ferrochromium

Fig. 2 (a) shows the final product after the completion of reduction process in a thermit reactor. The final product is conical in shape primarily due to the effect of tapering imparted by the inner lining of the refractory (Fig. 1). The metallic ferrochromium settles at the bottom due to its higher density as compared to the slag. It may be noticed from Fig. 2 (a) that the volume of the slag is much higher as compared to that of metallic ferrochromium. The metallic part is separated from the slag by hammering mechanically. The final metallic ferrochromium product is presented in Fig. 2(b). The size of the thermit product varies with the size of the reactor used in the process. The product will look like a pancake for pilot scale reduction. Fig. 3 represents the Back Scattered Electron image obtained from the surface of the ferrochromium chunk obtained from experiment no. 3 presented in Table 2. The EDS X-ray peaks obtained from analysing the selected area (spectrum 1) indicated the presence of Cr, Fe, Al and Si in the thermit product. The

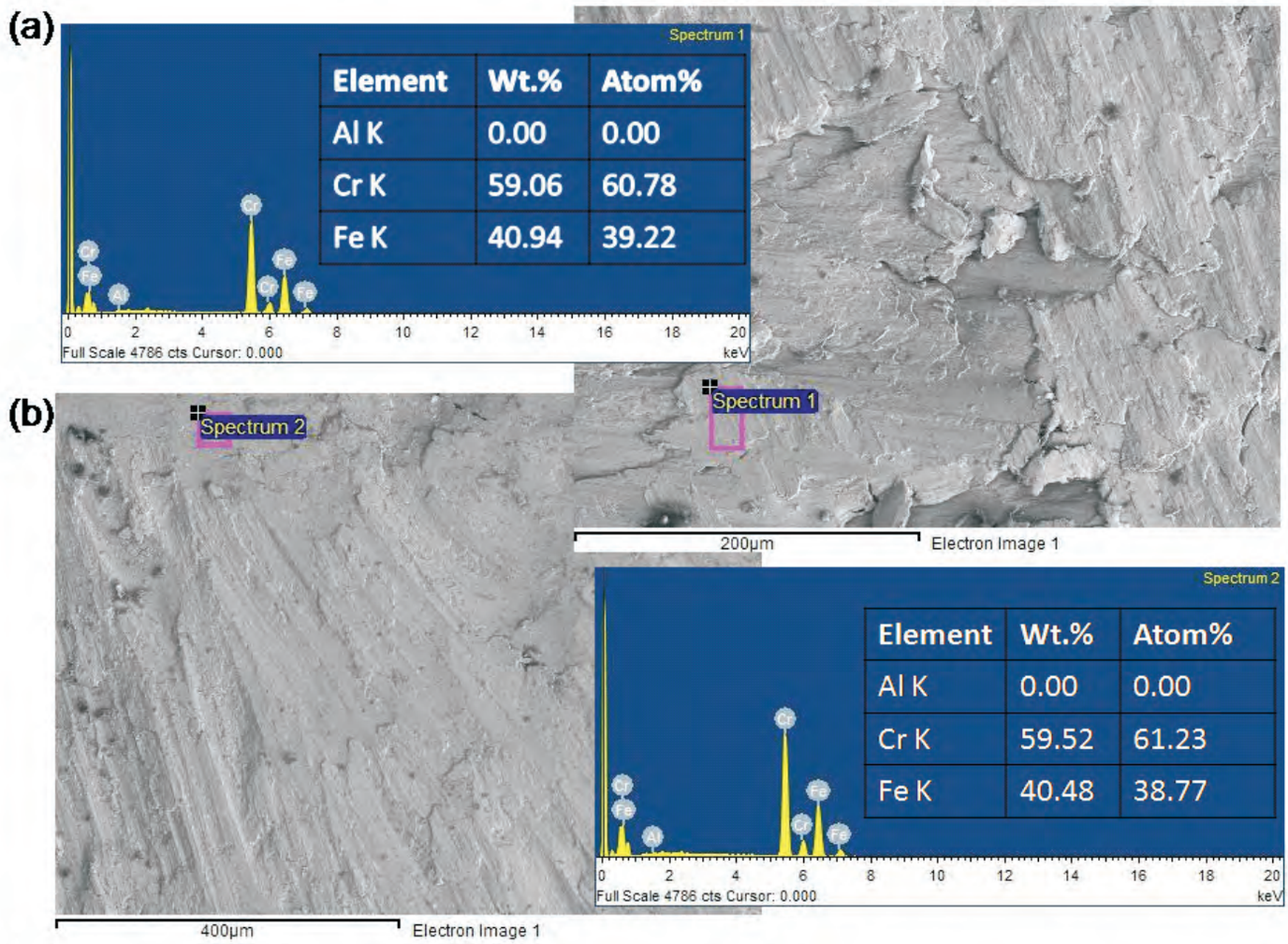

Fig. 4: SEM image, and EDS analysis of the ferrochromium obtained from Experiment No. 4 in Table 2

detailed chemical composition is presented in the table (inset) in Fig. 3. It may be noted here that the ferrochromium obtained from expt. 3 comprises of about 55 wt.% Cr, 3% Al, ~ 1% Si and the remaining is Fe. The carbon content in the product was found to be very low as no X-ray peak for C was detected in EDS analysis. Similarly, the higher amounts of impurity elements such as Al, Si etc. were present in the thermit ferrochromium obtained from the experiment nos. 1 and 2 (Table 2). High purity ferrochromium containing very low levels of Al or Si (~0-0.5%), and low carbon (0.02%) was obtained from expt. no. 4 in Table 2. Fig. 4 represents the detailed SEM and EDS analysis of the thermit ferrochromium product obtained from expt. no. 4. The EDS analysis carried out at different areas (Figs. 4a and 4b) of the metallic product indicated the presence of almost zero impurity (Al or Si) concentration. Near-targeted composition of about Fe-59.5 wt.% Cr was achieved from experiment no. 4 (Table 2). The same experiment was demonstrated in 800-1000 g scale, and the targeted ferrochromium composition was successfully achieved.

(b) Process optimization

Simultaneous reduction or coreduction of Cr_2O_3 and Fe_2O_3 by the reducing agent Al leads to the formation of ferrochromium in this process. The major reduction reactions in the thermit process are presented in the following.

$$Cr_2O_3 + 2Al \rightarrow 2Cr + Al_2O_3 \quad (1)$$

$$Fe_2O_3 + 2Al \rightarrow 2Fe + Al_2O_3 \quad (2)$$

$$3FeO + 2Al \rightarrow 3Fe + Al_2O_3 \quad (3)$$

$$6NaNO_3 + 10Al \rightarrow 3Na_2O + 5Al_2O_3 + 3N_2 \quad (4)$$

The enthalpy change (?H) of the above mentioned reactions dictates the progress of the thermit process. All the above reactions are exothermic in nature (showing negative change of the enthalpy). The ?H values for the reactions are calculated using the JANAF thermodynamic data table [5]. The reactions (1) and (2) are mainly responsible for the formation of ferrochromium (Fe-Cr) in the thermit melt. Reaction (3) is taken into consideration if some amount of FeO is already present either in the chrome

ore or in the mill scale. The exothermic heat generated from the reaction (4) is much higher as compared to that of the other three reactions. The composition of the thermit charge (feed) is formulated in such as a way that the overall heat generated from all the reactions is maintained in the range of 700-750 kcal per kg of the charge weight at 25°C temperature. The heat generated from reactions (1) and (2) is however lower as compared to these values. Consequently, addition of $NaNO_3$ (heat booster) to the charge helps to attain the optimal exothermic heat and also carry out the thermit process autogenously. Numerous experiments were conducted to optimize the composition of the charge for achieving good slag/metal separation, and for a superior yield of the thermit product. Table 2 represents some of the important results of the optimized composition of the charge which led to the good thermit yield. The maximum thermit yield obtained was about 72.5% with the highest possible Cr recovery of ~70%. It is also noticed from Table 2 that CaO as an additive could not improve the product yield. This detrimental effect of CaO is due to increase in viscosity and basicity of slag [4]. The viscosity of the slag increases rapidly with the solubility limit of calcium oxide exceeding in the alumina slag. Consequently, the metallic particles separation and settling is opposed, leading to a decrease in both metallic yield and chromium recovery. The other oxides such as MgO, SiO_2 etc that are present in the chrome ore join the slag phase along with the reaction product Al_2O_3. Therefore, the slag produced from the thermit process mainly comprised of alumina, having an overall composition of Al_2O_3-MgO-CaO-SiO_2. Some amount of unreduced Cr_2O3 and Fe_2O_3 also join the slag phase. However, detailed analysis of the slag composition may constitute the scope of further study. The results presented in Table 2 and in Fig. 4 clearly indicate that the desired ferrochromium (Fe-60Cr) alloy comprising low carbon and low Al content could be successfully produced by optimizing the parameters of the aluminothermy process.

Conclusion

Aluminothermic coreduction process was employed for preparing low-carbon ferrochromium with trace levels of aluminium. The composition of the charge comprising of Indian chrome ore and other additives, and the exothermic heat of the overall process were optimized. High quality thermit ferrochromium with a high metallic yield and high Cr recovery was successfully achieved. The process was demonstrated in 1 kg scale batches. This work is a part of the technology studies titled "Low-carbon Ferroalloys". The process know-how was transferred to M/s. National Ispat and Power Pvt. Ltd. (NIPPL), Bhubaneswar, India.

***Corresponding author**

Dr. Sanjib Majumdar

Acknowledgement

Authors are grateful to Mr. Rohit Pradhan, Director, National Ispat and Power Pvt. Ltd (NIPPL), Bhubaneswar, India for supplying Indian chrome ore. We convey our sincere thanks to Mr. S. K. Gavai, Mr. S. S. Molke and Mr. Ramdas Vanneldas of High Temperature Materials Development Section of MP&CED, BARC for providing technical assistance for carrying out thermit experiments.

References

1. V.I. Vasil'ev, M.A. Ryss, S.E. Pigasov, T.I. Petrova, Steel USSR, 6 (1976) 258-260.
2. O.S. Bobkova, O.K. Veretennikov, V.P. Nakhabin, A.A. Korolev, A.N. Shcherbin, A.Y.A. Brodskii, A.S. Gertner, Naryz, Stal, 8 (1969) 711-713.
3. A. Leško, E.Navara, Materials Characterization, 36 (1996) 349-356.
4. M.M. Eissa, K.A.El-Fawakhry, M.L. Mishreky, H.R. EI-Faramawy, The Twelfth International Ferroalloys Congress Sustainable Future, June 6-9, (2010), Helsinki, Finland, pp. 431-438.
5. M. W. Chase Jr., C. A. Davies, J. R. Downey Jr., D. H. Frurip, R. A. MacDonald, A. N. Syverud, JANAF Thermochemical Tables Third Edition, J. Phys. Chem. Ref. Data, Vol. 14, Suppl. 1, 1985.

Infrared Laser assisted Deactivation of Bacteria and Viruses

Tatsat Dwivedi, M.B. Sai Prasad, J. Padma Nilaya*
Laser & Plasma Technology Division, BTDG, BARC
Vandan Nagar, R. Shashidhar
Food Technology Division
A.V.S.S.N. Rao
Molecular Biology Division
S.K. Ghosh
Bio Science Group, BARC

Abstract

Exposure of bacteria and germs to electromagnetic radiation can lead to their neutralization/annihilation. In the present study, we have attempted to characterize the effect of pulsed CO_2 laser-assisted emission on the test samples consisting of bacteria and viruses. The laser source operates in the 10 µm region of the electromagnetic spectrum. The Aeromonas enteric bacterium and its specific virus, P2 bacteriophage, cultured on a typical matrix of Tryptic Soya Agar (TSA), served as the test samples. The agar overlay technique was used to examine the test results. Detailed analysis of the laser exposed samples showed complete neutralisation of bacteria and viruses for appropriate laser parameters.

Keywords: Laser assisted deactivation, Pulsed CO_2 laser, Tryptic Soya Agar (TSA), P2 bacteriophage Virus, Aeromonas Bacteria.

Introduction

It is widely acknowledged that under controlled conditions, electromagnetic radiation effectively neutralises bacteria and germs[1-3]. While gamma and UV radiation have the effect of degrading the genetic material of the organisms[4], exposure to infrared wavelength causes a rise in temperature which in turn results in their annihilation[5]. Excimer lasers and Infrared (IR) lasers, apart from material processing[6] have also been tried for decimating viruses[7-9] apart from bacteria. In the present study, we studied the effect of pulsed CO_2 laser emission on the enteric bacterium, Aeromonas, and its specific virus, P2 bacteriophage, grown on TSA matrix[10]. The mid-IR laser radiation is obtained from a pulsed TEA (transverse excitation atmosphere) CO_2 laser that operates in the 10 µm region of the electromagnetic spectrum. The efficacy of such a laser towards decimating the bacteria/virus and decontaminating surfaces by appropriately optimizing the process parameters viz., the laser power density, the pulsing frequency etc., has been studied.

Laser as a Decontamination Tool

The conventional methods of surface cleaning, viz., mechanical and chemical methods are mostly abrasive in nature, whereas, manual methods are labour-intensive. Laser assisted surface decontamination has gained popularity in semi-conductor industry[6,7], nuclear industry[11,12] and conservation industry[13] etc., over last several years mainly because of the following inherent advantages.

1. The process can be well controlled. The laser parameters can be so chosen as to systematically remove the contamination across each layer without damaging the substrate surface.
2. The process can be made remote.
3. The waste generated can be minimised as compared to any other method.

The effect of laser beam on the surface depends on the extent of its absorption, which in-turn depends on the wavelength of the laser emission. A representative curve of absorption for both metals and dielectrics as a function of wavelength of the incident light is shown in figure 1. The absorption is via electronic excitation in UV, VUV regions, electronic excitation and inverse-Bremsstrahlung (IB) in the visible region, multi-photon absorption in the near-IR region and vibrational excitation and feeble IB in the mid IR region. This absorption, in the IR region, results in rise of the surface temperature and is a function of the intensity and pulse duration of the laser. In case of irradiation with continuous wave (CW) or long pulses (ms duration) of appropriate intensity, the resulting surface temperatures can be high enough to cause melting effect, leading to the possibility of cutting and welding[6,8]. As the pulse duration reduces to micro seconds, as is the case with a TEA CO_2 laser, the

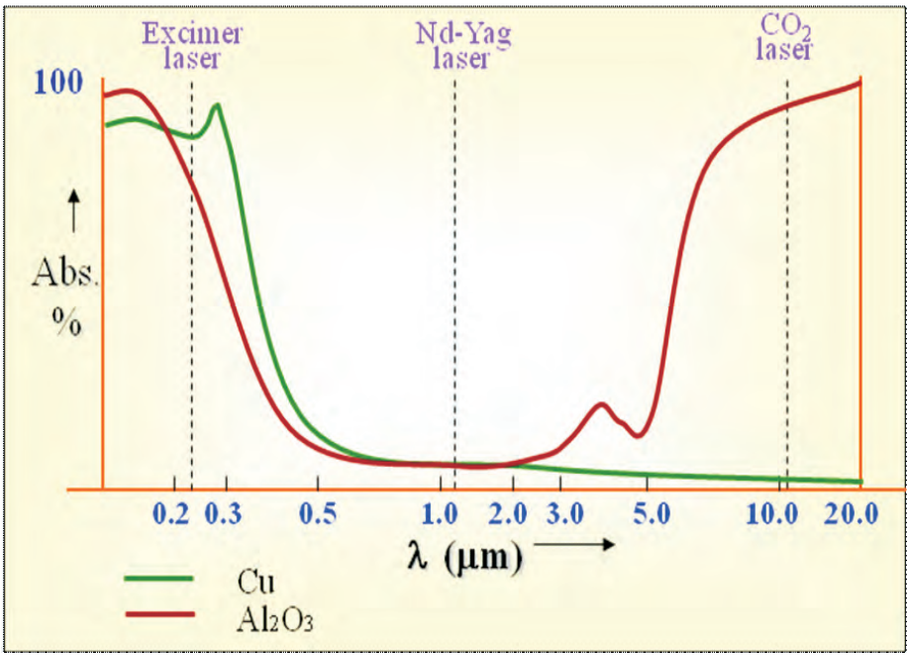

Fig. 1: Depiction of % absorption as function of emission wavelength for metal and dielectric materials

transfer of high energy over such short duration can increase the surface temperature so much so as to even cause vaporisation[6,8]. The depth of penetration and the conduction of heat into the bulk can be reduced further by making use of nano-second and pico-second duration pulses[6,8].

Experimental Work

a) Sample Preparation/Description

Two types of samples, those of bacteria and virus, were prepared as described below.

The enteric bacterium Aeromonas (10^7cfu/ml) was grown on Tryptic Soya Agar (TSA) matrix[10]. TSA contains digests of casein and soybean meal. The combination of casein and soy peptones renders the medium nutritious by supplying organic nitrogen, particularly amino acids and longer-chained peptides. Sodium chloride is added to maintain osmotic equilibrium and agar acts as solidifying agent. One litre of agar contains15 gm tryptone, 5 gm soytone (enzymatic digest of soybean meal), 5 gm sodium chloride and 15 gm agar.

P2 phage (lab isolate) is a bacteriophage (virus) of Aeromonas hydrophila CECT 839^T. It was isolated from the sewage treatment plant located in Anushaktinagar, Mumbai. Since P2 phage is not pathogenic to humans, it does not require services of special microbiology laboratory to handle it. The P2 phage was propagated using A. hydrophila CECT 839^T as host. 1 ml of overnight grown A. *hydrophila* CECT 839^T culture was added to 25 ml tryptic soya broth, TSB (2 mM $CaCl_2$) and kept at 30°C on shaker. At 0.3 O.D. (3 x 10^8 cells/ ml), 500µl of the P2 lysate (1 X 10^9 pfu/ml) was added to A. *hydrophila* CECT 839^T culture and incubated at 30°C for 30 minutes without shaking the mixture. The culture was grown at 30°C with vigorous shaking till lysis occurred (3-4 h) and 0.2% v/v chloroform was added to the broth followed by shake-incubation for 10 min. The broth was centrifuged at 10,000 rpm for 10 min at 4°C, followed by addition of 0.1% chloroform to the supernatant and stored at 4°C.

Samples of P2 phage were also taken in a liquid form that was prepared by suspending the virus sample (P2 bacteriophage) in a solution containing NaCl+$MgSO_4$ buffer solution, NaCl:100 mM, $MgSO_4.7H_2O$:8 mM; Tris-Cl 50 mM (pH 7.5).

b) Analysis of post-irradiated samples

The effect of laser on survival of P2 phage was assayed using the agar overlay technique. 100 µl of appropriately diluted (10^6 pfu/ ml) P2 phage was spread on Tryptic Soya Agar (TSA) plates. 100 µl of A. *hydrophila* CECT 839^{T}cell suspension (10^8 cfu) was added to 3 ml, 0.7% molten agar and was poured on TSA-2 mM $CaCl_2$ plates. These plates were incubated at 30°C for 24 hours and the formation of plaques was observed. Later, these were analysed for the presence or absence of virus following the growth of bacteria.

c) Laser irradiation of samples

A pulsed CO_2 laser (Light Machinery, Canada) operating on 10.6 ì m wavelength, capable of delivering ~2 J/pulse, pulse repetition frequency ranging from 1-100 Hz acted as the source. A schematic of the

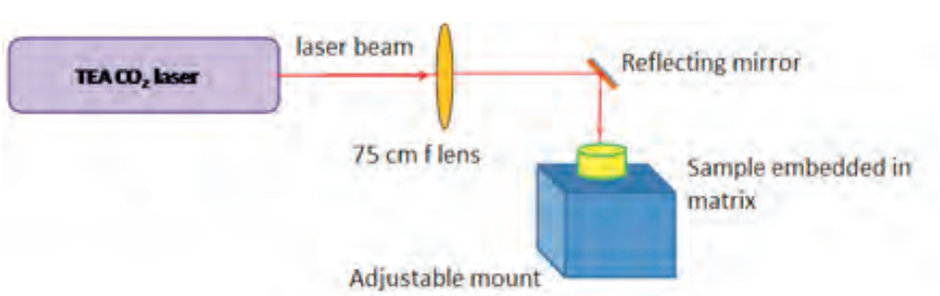

Fig. 2: Schematic Diagram of the experimental set-up

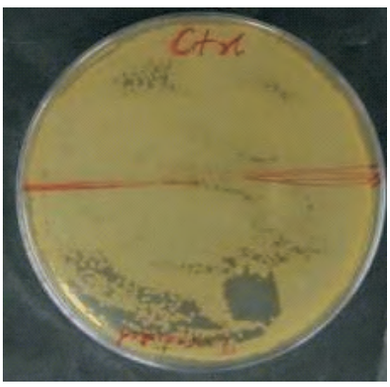

Fig. 3: Co_2 laser irradiation of Aeromonas (10^7cfu/ml) grown on Tryptic Soya Agar matrix

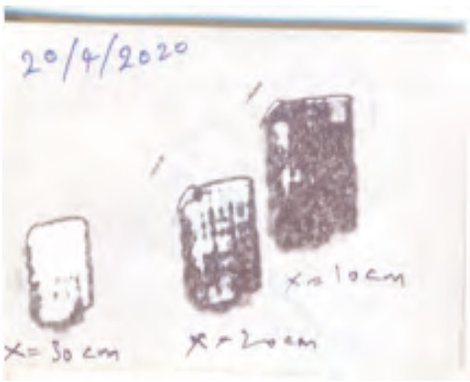

Fig. 4: Impression of laser beam on a sensitive thermal paper at various distances from the lens

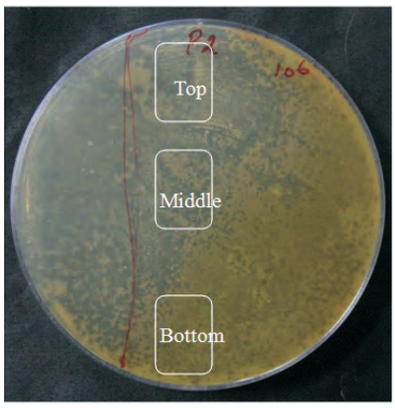

Fig. 5: Effect on virus grown on TSA matrix for 1 (top), 5 (middle) and 10 (bottom) exposures (table 2). Growth of bacteria in the bottom trace indicates more effective killing of virus

experimental set-up is shown in figure 2. Focusing lens was used to gradually increase the laser intensity on the sample plane, and the same was estimated by measuring the beam size at the target location and the laser energy.

In the first set of experiments, four different sets of bacterial samples were irradiated at different laser intensities and were analysed (table 1). No bacterial growth is expected to be observed in the laser-exposed zone in the event of its annihilation while normal bacterial growth is expected in the other regions. For the samples irradiated at different laser conditions as described in table 1, no killing of the bacteria could be observed for the cases of samples 1, 2 and 3 except for sample 4, where broad-based killing of the bacteria upon exposure to laser at ~0.4 J/cm² (1.824 J over an area of 25 mm x18 mm) could be observed for a repetition rate of 30 Hz as shown in figure 3. The top half of figure 3 indicates the control standard (no laser exposure) while the bottom half indicates the irradiated region at 0.4 J/cm², 30 Hz. Thus, it is clear from table 1 that the laser irradiation of the samples under unfocussed condition (i.e., lowest fluence) but with an increased repetition rate (30 Hz) and an exposure time of 1 sec inhibited the growth of bacteria. Further, it was observed that the matrix was intact during the process. It may be noted that the increased temperature effect at higher laser fluence may also be achieved at lower fluence but at higher pulse repetition rate due to inefficient heat conduction between pulses. Impressions of the laser beam on a thermal sensitive paper at various distances from the lens towards arriving at the incident intensities are as shown in figure 4.

In the second set of experiments, virus samples, viz., P2 bacteriophage, at a concentration of 10^6 pfu/ml, were exposed to laser pulses of different intensities viz., 0.535 J/cm², 0.764 J/cm² and 1.2 J/cm² (as enumerated in table 2). The irradiation was carried out with the pulsed CO_2 laser emission at 3 different regions of the prepared samples, i.e., at the top, middle and the bottom regions. A sample case is shown in figure 5 for ease of understanding. In order to test the effect of the irradiation on the virus samples, the same have been exposed to *Aeromonas* bacteria post irradiation. It can be observed from table 2 that, only for case of irradiation at 1.2 J/cm² (sample 3), the virus could be most effectively killed indicated by the presence of bacterial growth (in the bottom region as indicated in figure 5) and no such growth in the other regions (top and middle) where the

Table 1. Irradiation of bacterial samples with CO_2 laser (10.6 μm)

Sample	Focal distance	Laser Fluence	Irradiation conditions	Inference
1st	60 cm	4.3 J/cm^2	5 pulses, 1Hz	Bacterial growth is inhibited
2nd	30 cm	1.2 J/cm^2	5, 10 pulses, 1Hz	Bacterial growth is inhibited
3rd	10 cm	0.5 J/cm^2	20 pulses, 1Hz	Bacterial growth not inhibited
4th	0	0.4J/cm^2	Control (standard) (top half) Bottom (30Hz, 1 sec)	Growth present Growth inhibited

Table 2. Irradiation of virus samples with CO_2 laser (10.6 μm) at different fluences.

Sample	Virus density (pfu/ml)	Focal distance	Laser Fluence	Region of irradiation	Inference
1st	10^6	10 cm	0.535 J/cm^2	Top (1 pulse, 1 Hz) middle (5 pulses, 1 Hz) Bottom (10 pulses, 1 Hz)	No observable killing of virus
2nd	10^6	20 cm	0.764 J/cm^2	,,	Partial killing of virus
3rd	10^6	30 cm	1.2 J/cm^2	,,	-* ++* +++* Ablation of matrix observed

* + indicates effectiveness of virus decimation. Qualitative comparison of virus killing as shown in Figure 5.

Table 3. Irradiation of virus samples with CO_2 laser (10.6 μm) for different exposure times; Laser fluence = 0.764 J/cm^2, 1 Hz repetition rate.

Sample	Virus density (pfu/ml)	Focal distance	Exposure time	Killing of virus
1st	10^5	20 cm	1 sec	+/-
2nd	10^5	20 cm	5 sec	+/-
3rd	10^5	20 cm	10 sec	+
4th	10^5	20 cm	15 sec	++

+/- denotes the very marginal killing of virus; + denotes more killing of the virus as compared to +/-; ++ denotes more killing of the virus as compared to +.

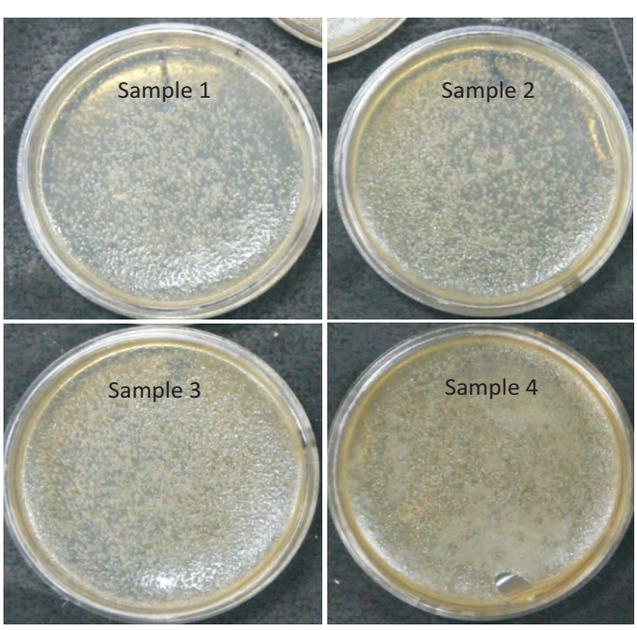

Fig. 6: Gradual increase in decimation of virus visible in samples 1 to 4 as number of exposures increased (table 3)

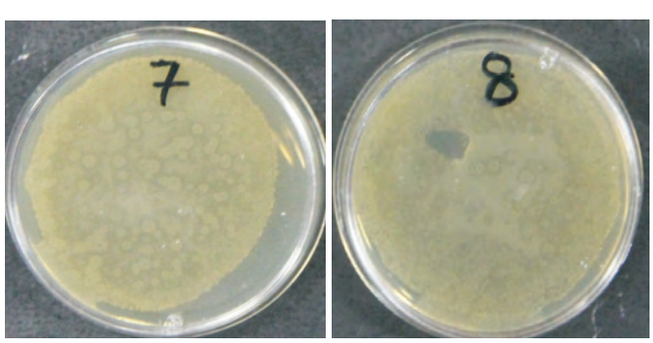

Sample 7 **Sample 8**

Fig. 7: Increased repetition rate at the same fluence resulted in matrix damage in sample 8

virus was not affected by laser radiation. Partial killing of virus resulted in partial growth of bacteria (figure 5, middle region).

More detailed studies were carried out with samples irradiated with higher number of laser pulses and at higher repetition rates. In this regard, firstly the four samples, viz., sample 1, 2, 3, 4, as shown in figure 6, were irradiated at a constant fluence of 0.764 J/cm^2 (table 3). The photographs shown in figure 6 are actually of the samples one day following the laser exposure. The clear gradation of the growth of bacteria and hence improved efficiency of virus decimation with increased number of laser pulses is evident for irradiation conditions as tabulated in table 3. To be noted, the medium remained intact in the entire process.

Following this, two more samples, viz., samples numbered 7 & 8 (figure 7) have been irradiated at a fixed fluence of 0.535 J/cm^2 but at 1 Hz and 10 Hz repetition rate respectively. A zone of matrix damage could be seen for the case of irradiation at 10 Hz (as can be seen in figure 7) owing to rise in surface temperature.

In the last set of experiments, the virus sample (P2 bacteriophage) suspended in a liquid medium (NaCl+$MgSO_4$ buffer solution; NaCl:100mM, $MgSO_4.7H_2O$:8mM;Tris-Cl (50 mM, pH 7.5) was exposed to laser radiation at 0.535 J/cm^2. However, this did not result in any observable killing of the virus.

Conclusion

The effect of mid IR laser radiation on the bacterial and virus samples has been investigated and the results summarized. We observed that the extent of bacterial killing increased either with increased laser fluence (0.4 to 1.2 J/cm^2) or with increased number of pulses (1 to 30) and increased repetition rate. Even though the extent of P2 bacteriophage killing also showed similar trend, the effect is much less distinct. Importantly, the matrix in which the viruses are suspended seems to play a significant role. Viruses suspended in a liquid medium showed little or no killing, perhaps due to the localized evaporative heating of water and little heating of the bulk of the medium. The results obtained from the present study provide a qualitative evidence for killing of viruses by CO_2 laser. A more elaborate study is needed to identify exposure conditions for optimum killing of viruses.

***Corresponding author**

Dr. (Smt.) J. Padma Nilaya

Acknowledgement

The authors sincerely acknowledge Dr. Archana Sharma, Associate Director, Beam Technology Development Group (BTDG) for initiating this work and for her constant guidance and support throughout the study.

References

1. Effect of UV and Gamma irradiation sterilization processes in the properties of different polymeric nanoparticles for biomedical applications,Y. S. Tapia Guerrero, Materials (Basel), 13(5), 1090 (2020).
2. Germicidal effect of ultraviolet Irradiation on paper contaminated with mycobacteria.T. W. Huber, Applied Microbiology, 19 (2), 383-384 (1970).
3. Comparative radiation death kinetics of clostridium botulinum spores at low temperature gamma irradiation, A. Anellis, D. Berkowitz, and D. Kemper, Journal of Food Protection, 40, 313-316(1977).
4. Bactericidal efficacy of carbon dioxide laser against bacteria-contaminated titanium implant and subsequent cellular adhesion to irradiated area,T Kato et al., Lasers in Surgery and Medicine 23, 299-309 (1998).
5. Biological effects of sunlight, ultraviolet radiation, visible light, infrared radiation and vitamin D for health. Michael F Holick, International journal of cancer research and treatment, 36(3), 1345-56 (2016).
6. Laser material Processing, William M. Steen, 4th edition, Springer.
7. Pulsed light for food decontamination: A review, Vicente M. Gomez-Lopez, Trends in Food Science & Technology, 18, 464-473 (2007).
8. High power lasers in production engineering, Dieter Schuocker, World Scientific Publications Co. Inc. (1999).
9. Factors affecting the antibacterial effects of Nd:YAG laser in vivo, GokceMeral, Lasers in Surgery and Medicine 32, 197-202 (2003).
10. https://en.wikipedia.org/wiki/Tryptic case Soy Agar.
11. https://alliedscientificpro.com, nuclear-decontamination by laser for decommissioning.
12. High-power fiber laser cutting parameter optimization for nuclear decommissioning, Lopez AB, Nucl. Eng. Technology, 49, 865-872 (2017).
13. Lasers in the Preservation of Cultural Heritage: Principles and Applications, Vassilis Zafiropulos, Physics Today (2007).

Experimental and Theoretical studies of Multi wavelength Dye Laser System

G. Sridhar*, Paramjit Rana, Sandeep Kumar Agarwalla, Jaya Mukherjee
Laser & Plasma Technology Division, BARC

Abstract

Multi wavelength dye lasers find applications in atmospheric probing studies, resonance ionisation spectroscopy, gas sensing and trace analysis. Reports on independently wavelength tunable and narrow bandwidth multiwavelength dye laser with three or more colours is scarcely available. In this study, we report experimental studies and demonstration of generation of two to five wavelength laser operations from a single dye laser cavity. Gain competition effect of all the sub-cavities was characterized in detail. Theoretical study on the generation of multi wavelength in a cascaded grazing incidence grating cavity (CGIG) laser cavity and multi wave amplifier was carried out to study the gain competition effects among the lasing wavelengths.

Keywords: Multi wavelength dye lasers, Multi wave Laser Oscillator, Resonance Ionisation Mass Spectrometry (RIMS), Cascaded Grazing Incidence Grating Cavity (CGIG), Gain Competition Effect.

Introduction

Resonant ionization mass spectrometry (RIMS), atomic vapour laser isotope separation (AVLIS), multi wavelength light detection and ranging (LIDAR), gas sensing and trace analysis require a spatially overlapped, independently wavelength tunable, narrow linewidth laser beams at 3 or 4 wavelengths. Conventionally, these lasers are generated in separate dye oscillators and are successively amplified to the desired power levels and optically combined. This makes the laser facility complex. Further difficulty in achieving optimum spatial overlap is caused by the unequal aspect ratio of the different beams from different laser chains. As an alternative to this approach, we built a compact laser system where a single oscillator will generate the required multiple wavelengths simultaneously with a single spatially overlapped collinear output beam. Subsequently, composite laser beam may be amplified through common amplifier stages to boost the power level to the required value.

Many authors had demonstrated the dual wavelength operation of dye laser by employing various intracavity optical elements and techniques. Nair et al.[1] had reported the double wavelength generation from a grazing incidence tunable dye laser without intra cavity beam expander. However, studies on triple and four wavelength generation from dye laser are scarce. Recently, Khare et al.[2] had reported three wavelength operation from copper vapour laser pumped Rh6G dye laser. Two out of three wavelengths were independently tunable and their spectral widths were of the order of $0.3cm^{-1}$ (9 GHz). Simultaneously operable, independently tunable, collinear, three and four wavelength dyelaser is first time reported from our lab[3]. Configurations with inherent narrow linewidth generation capabilities were selected. Gain competition plays a significant role in dictating the intensity ratio, tuning range and sustained multiple wavelength operation for collinear output generation in a homogeneously broadened gain medium.

In order to understand the temporal evolution dynamics of each laser sub cavity, we have carried out theoretical studies of time dependent multi wave oscillator by solving time dependent rate equations extending our earlier work[4]. The effect of gain competition and the build up time of each laser signals were studied in detail for the first time for three wave length resonator. Experimental study of high repetition rate copper vapor laser pumped dual wave dye amplifier has been reported earlier by Sunita Singh et al.[5] and recently by our laser group[6]. No theoretical studies on multiwave dye amplifier to study the gain competition are reported earlier. We present a generalized theoretical study of two and three wave amplifier and their gain competitions based on the rate equations[7].

Description

In this work, we have chosen dye laser cavities for our study, which has inherent capacity to generate narrow bandwidth emission with wavelength tunability. Fig.1 shows a cavity for generating dual wavelength from hybrid twin prism expander (PBE) based grazing incidence cavity. Grating has 2400 lines/mm groove density and angle of incidence was maintained at 81 degrees with PBE magnification of 22X. Zeroth order output of Grating1 was used for second lasing with Grating-2 and tuning mirror (TM2) pair. Pump laser used in this experiments was 20 Hz

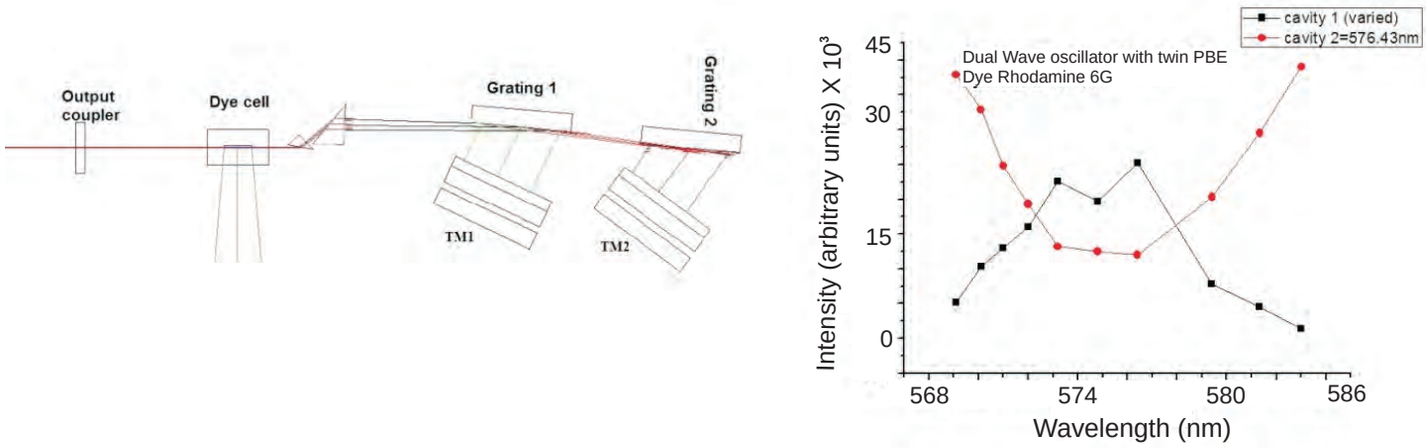

Fig. 1: Schematic of dual wave dye laser and gain competition effects of wavelength tuning

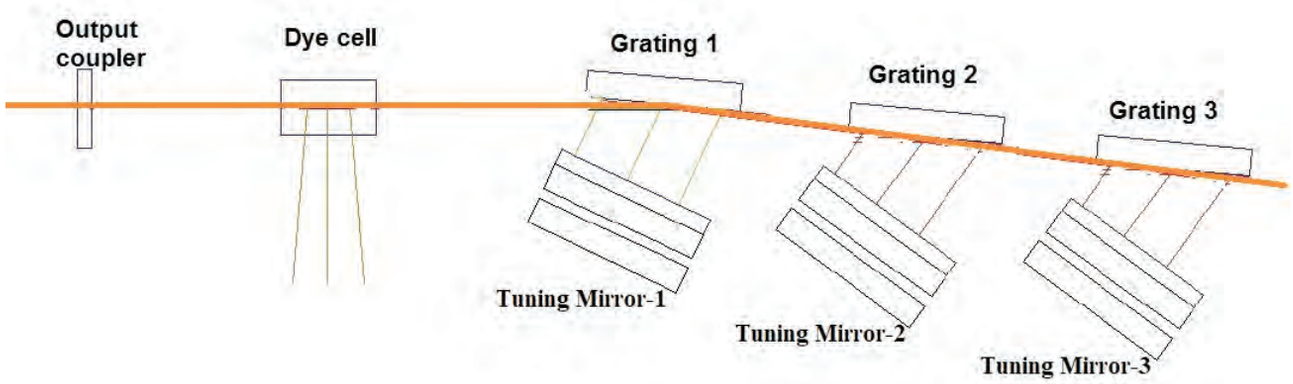

Fig. 2: Schematic of three wave laser cavity

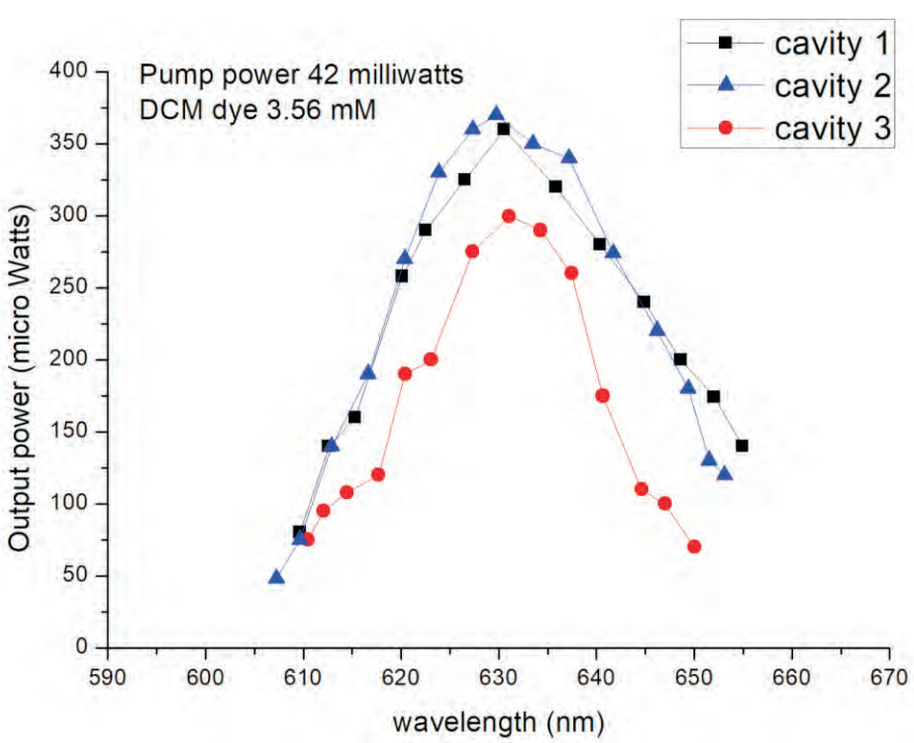

Fig. 3: Tuning range of individual cavities

second harmonic Nd:YAG laser. Pulse energies were kept in the range of 1-2 milli joules. Concentrations of dye and dye mixtures were optimised so that 70% of light absorbed in 100 micron as suitable for single sided transverse pumping. Cavity 1 is comprised of Output Coupler-Dye Cell-PBE-Grating 1-TM1 and cavity 2; output coupler-Dye cell-PBE-Grating 1-Grating 2 –TM2 respectively.

Fig. 1 also shows the gain competition among the two wavelengths for rhodamine 6G dye laser. Wavelength of cavity 2 was fixed at 576.4 nm at the peak of the gain and the wavelength of cavity 1 was varied and the effect of wavelength tuning of cavity1 on the intensity of cavity 2 with fixed wavelength clearly shows gain competition effect which is expected to occur as both laser cavities share common gain medium.

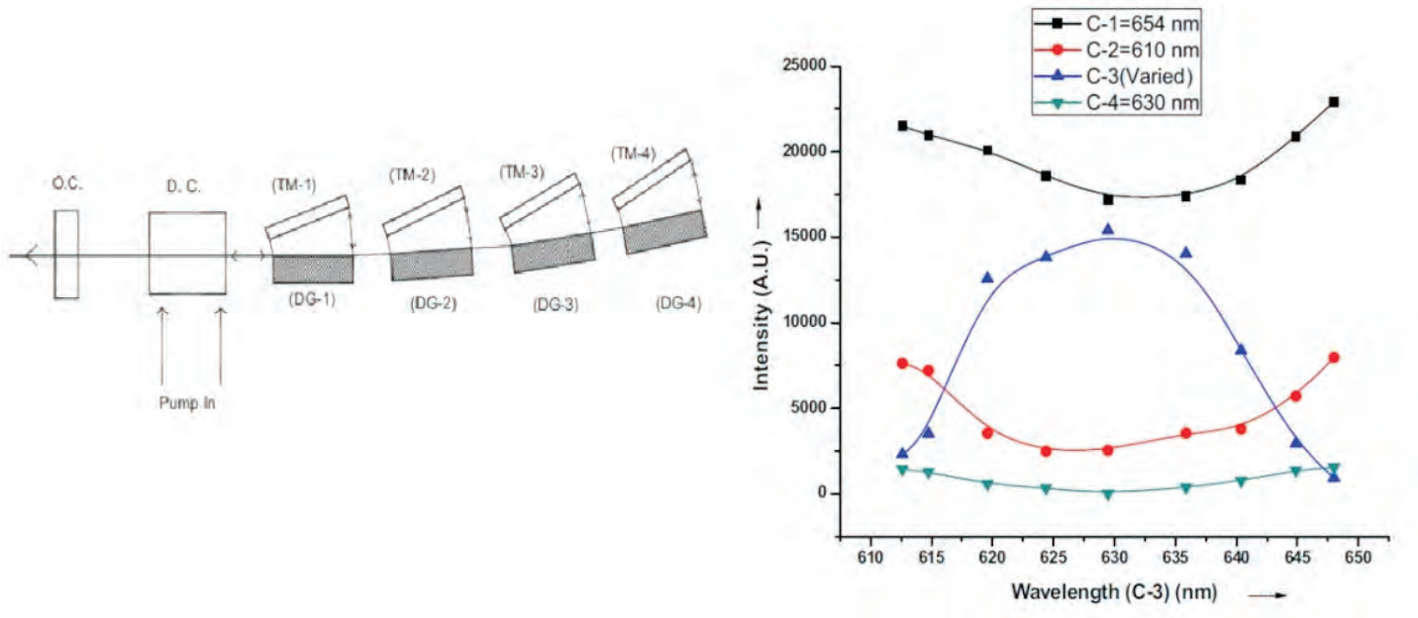

Fig. 4: Four wave CGIG cavity and the gain competition effect of wavelength tuning of C3

In order to generate three and more wavelengths, intra cavity losses have to be reduced to a minimum value. Fig. 2 shows the cavity of three wave lasing demonstrated in our lab. Advantage of this cavity is no additional intra cavity expanders and grating is kept at high AOI. Diffraction efficiency at first order at ~ 880 is less than 5% and only part of gain will be used for lasing at cavity 1. The inset of Fig. 2 shows simultaneous lasing at three wavelengths at 620 nm, 630 nm and 637 nm respectively as seen in spectrometer.

Fig. 3 shows tuning range curve of individual cascaded GIG cavity for DCM gain medium. Here grating is kept at ~ 890 AOI and the grating efficiencies at the first order are ~ 1-2 %. By reducing grating illumination length from 62 mm to 52 mm, peak efficiencies were increased to 2-3%. The spectral width at this illumination lengths were measured to be 2 GHz, 3 GHz and 4 GHz respectively for cavity 1 and cavity 2 and cavity 3. The increase in line width was attributed to increased round trip time from cavity 1 to cavity 3 and shorter pulse width (8ns) of Nd:YAG Laser.

We have extended this work on three

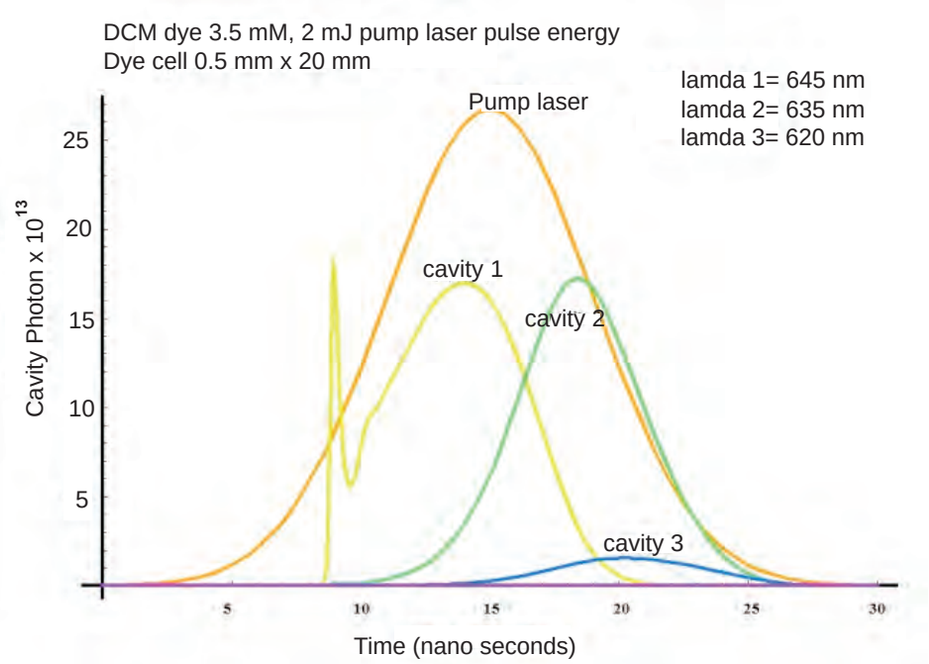

Fig. 5: Theoretical simulation of three wave CGIG dye laser

wave laser to four and five laser by adding additional Grating and tuning mirror and reported for the first time. Fig. 4 shows the four wave cavity demonstrated in our lab. This casacded grazing incidence grating cavity (CGIG) was successfully achieved in DCM dye gain medium. Detailed cavity characteristis of individual cavities such as temporal and spectral parameters were carried out. The effect of cavity wavelength tuning on other cavity power out put was studied in detail.

Fig. 4 shows the effect of wavelength tuning of sub cavity 3 formed by OC-DC-DG1-DG2-DG3-TM3 on other sub cavity's laser output. Here wavelength of cavity 1 and cavity 2 and cavity 4 were fixed at 654 nm, 610

nm and 630 nm. Similar studies were carried out for each sub cavity and this resulted in the identification of wavelength domain of each sub cavity for simultaneous four-wavelength operation. We have also demonstrated simultaneous five wave length laser operation with adding additional grating after DG4 in a littrow configuration[3].

Theoretical study of Multiwave laser oscillator

Recently theoretical study of gain competition in dual wave oscillator with different polarization was described[8]. The above work was based on the steady state analysis and other temporal details of build-up time and the pulse shapes will not be explained and limited to two wave oscillator.

In order to understand the temporal photon dynamics in a three wave CGIG cavity, our earlier study on single mode dye laser cavity was extended with incorporation of gain competition among lasing signals[4]. This new study is based on the time dependent rate equations of four level dye laser and laser cavity photon evolution. Fig. 5 shows the three wave dye laser simulation based on DCM gain medium and SHG of Nd:YAG laser with Gaussian temporal profile as the pumping laser. The parameter such as gain volume and cavity length and other parameters were maintained similar to our reported work on multiwave laser system[4]. Wavelength of cavity 1 was kept at 645 nm and wavelengths of cavity 2 and 3 were kept at 620 nm and 635 nm respectively. In this case, cavity 1 has relatively lower loss compared to other cavities and as the gain crosses the cavity 1 threshold, most of the the gain utilized in generating photon in cavity 1and generating an initial sub nanosecond spike. This is also seen in the excited state population temporal dynamics. Initial spikes in dye laser were also reported in high loss cavity

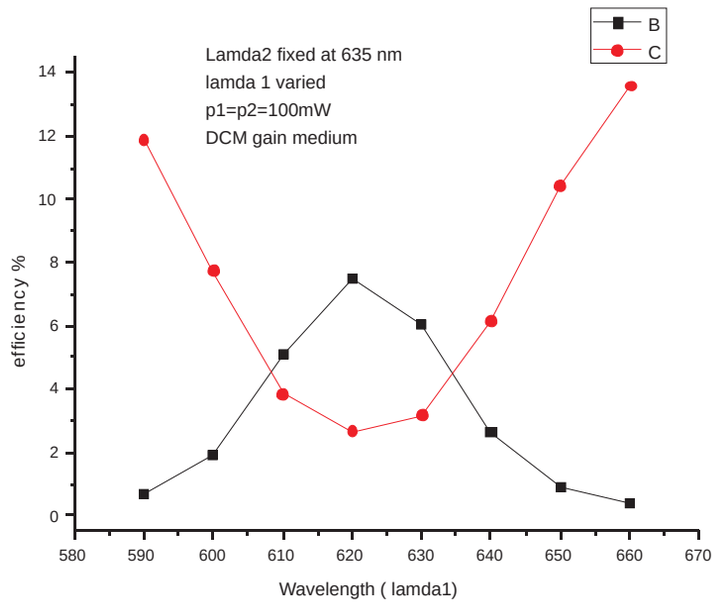

Fig. 6: Effect of wavelength tuning of DWA

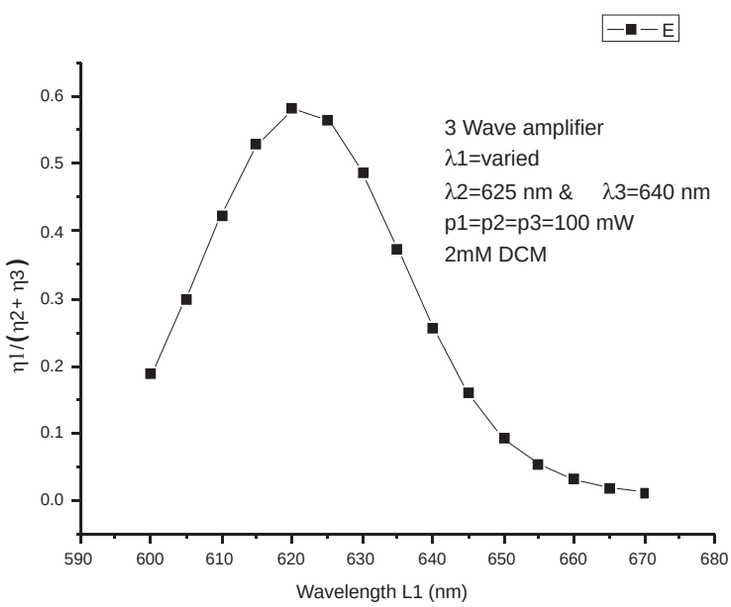

Fig. 7: Three wave amplifier gain competition

and attributed to relaxation oscillation[9]. This was utilised for generating sub nanosecond pulses in the early development of shorter dye laser pulse. The efficiency of grating was assumed to be 5% for GIG at large AOI. Further work is being carried out to extend to four wavelength and their gain competition effects among lasing wavelengths.

Theory of multi wave dye amplifier

The theoretical study of generic multi wavelength pulsed dye amplifier based on the gain characteristics of dye amplifier and the results for dual and three wave amplifier is presented. The gain extraction of pulsed dye amplifier can be estimated by relevant four level steady state rate equations. Presence of two dye laser signal beams inside the dye amplifier modifies the gain extraction dynamics. As the dye is excited from ground state to an upper state by the pump beam, both signal beams compete with each other to extract gain available from common excited state population. The relevant

rate equation based on steady state in time and spatially varying gain extraction for generalized three wave amplifiers with gain competition effects was arrived and evaluated[7].

In our study we have taken transversely pumped gain medium with dimensions of 10 mm x 0.5 mm x 0.5 mm. Fig. 6 shows the effect of the wavelength tuning of signal 1 on the gain extraction on both wavelengths for DCM gain medium for dual wave amplifier. Here Lamda 2 is fixed at 635 nm. Dual wave amplifier theory was extended to three wave amplifier, where three signals are simultaneously competing for the gain in the dye amplifier. Fig. 7 shows the result of three wave amplifier simulation here amplifying signal wavelengths were fixed for signal 2 and signal 3. Gain competition coefficient of signal 1 is defined as the ratio of its efficiency with the sum of other two signal's efficiencies. Gain coefficient smoothly increases from 0.19 to 0.56 as the wavelength varies from 600 to 625 and afterwards decreases closer to zero as the wavelength increases beyond 625 nm.

Conclusion

We have presented the development of narrow band, wavelength tunable multi wave laser with 2 to five wavelength generation from a single cavity along with the gain competition studies and identification of wavelength zones of each cavity for multi wave operation. Theoretical study of dual and three wavelength oscillator and amplifier based on four level rate equations are reported. Multi wave dye oscillator and amplifier system and gain competition can be optimized on signal with a good choice of dye solvent and mixture for oscillator and amplifier systems.

***Corresponding author**

Dr. G. Sridhar

Acknowledgement

The authors would like to express their sincere gratitude to Dr. Archana Sharma, Head, Laser and Plasma Technology Division, BARC for her interest and encouragement for this work.

References

1. L.G. Nair, K. Dasgupta, IEEE J. Quantum Electron. 16 (2), p111 (1980).
2. R. Khare S.R. Daulatabad H.S. Vora R. Bhatnagar Opt. Commun. 114, pp275–279 (1995)
3. Paramjit Rana, G.Sridhar, K.G.Manohar, 86, pp39-45 J.Opt. Las. Tech (2016)
4. G.Sridhar,V.S.Rawat, S.Singh, L.M.Gantayet, "Temporal dynamics of high repetition rate pulsed single longitudinal mode dye laser" Pramana, Journal of Physics, Vol 81, p295, 2013.
5. Sunita Singh, K.Dasgupta, Sasi Kumar, L.G.Nair, U.K.Chatterjee "Dual wavelength dye laser amplifier" Opt.Comm., 78, p 373 (1990)
6. Paramjit Rana et al, "Co-amplification: An efficient spectral beam combination approach for high power, closely separated dual Wavelength dye laser systems" Opt.Commun. , 451, P367 (2019)
7. S.K.Agarwalla, G.Sridhar, "Theoretical study of multiwavelength dye amplifier" Optik- International Journal for Light and Electronics, 199, 163323 (2019)
8. S.Jelvani, B.Khodadoost, "Gain competition effects in dual wavelength dye laser", J.Opt. Las.Tech. , 39, p182 (2007)
9. C.Lin, "Studies of relaxation oscillation in organic dye lasers" IEEJ.QE, 11, p602, 1975.

Indigenous synthesis of Organic-Inorganic Scintillator Materials for Radiation Monitoring

O.D. Jayakumar*, Adish Tyagi, A.K. Tyagi*
Chemistry Division, BARC
Anand Raman, A.K. Chikara, Govinda Mukherjee, Ashutosh Gupta, Probal Chaudhury
Radiation Safety Systems Division, BARC

Abstract

This report presents the development of prototypes of gamma radiation survey/Dose rate meter, contamination monitors of alpha/beta/gamma, gross beta, and gamma detectors. A new organic scintillator film of micron thickness is developed for tritium detection with enhanced sensitivity. The objective was to incorporate indigenously synthesized scintillation materials in radiation monitoring systems developed in BARC. These would serve the broad aim of providing a substitute for the otherwise imported radiation measurement systems. The in-house developed plastic scintillation detectors were found to reflect an intrinsic interaction efficiency and scintillation efficiency, comparable with that of the commercially procured detectors. The prototype of gamma radiation survey/Dose rate meter has been field tested for routine operation in nuclear facilities. The performance of the system has been found as acceptable for regular usage. The detectors that have been incorporated in to the survey meters have remained consistent in response for a period of more than 4 years. The initial prototype designed and developed showed a linear dose rate response from background of 50 nSv/h to 20 mSv/h. Preliminary studies of the response of the contamination monitor prototype system on exposure to beta particles emitted from $^{90}Sr/^{90}Y$ source provided detection efficiency of the order of approximately 25% and alpha particle detector tested using ^{241}Am source showed ~25 % of efficiency. Micron thick scintillator for tritium has been tested and found to be about ~ 15 times better than the current scintillator films used for the same purpose.

Keywords: Plastic scintillator, Gamma dose rate meter, beta detector, tritium detector, alpha detector.

Introduction

Radiation monitoring is an important component which supports radiation surveillance and safety program in all nuclear facilities associated with all aspects of the nuclear fuel cycle. The primary objective of this program is to minimize personnel radiation dose to working personnel. This program entails systematic and regular radiation monitoring in the environment neighbouring nuclear facilities for detecting fall out, if any, of the operation of the nuclear facilities in the public domain. The detectors used for survey and contamination monitoring include gas filled radiation detectors and scintillation detectors. Presently, most monitoring systems employ the scintillation detectors as compared to the gas filled radiation detectors due to the higher sensitivity and ease of usability of the scintillation detectors. Although applications for alpha and beta measurements which necessitate better gamma discrimination capabilities are better served by gas filled radiation detectors.

Scintillation detectors are broadly classified as organic and inorganic based. The inorganic scintillation detectors such as NaI(Tl), CsI(Tl) etc., are primarily used for pulse height analysis and the subsequent radionuclide identification. However, these detectors are limited in terms of the sizes that can be fabricated out of them and are also characterized with significantly longer decay times. In addition, these detectors are relatively expensive as compared to organic scintillation detectors. Organic scintillation detectors do not qualify for measurements related to radionuclide identification due to their low Z values resulting in poor photoelectric interaction efficiency. Nevertheless, organic scintillation detectors qualify as the best choice for radiation monitoring applications that do not require radionuclide identification such as routine radiation survey measurements and contamination monitoring. Plastic scintillators, which are the subject of the present discussion, belong to the category of organic scintillation detectors. The advantages of plastic scintillation detectors include low cost, fairly high light output and shorter decay time of 8-10 nanoseconds. Another advantage of plastic scintillation detectors is their ability to be shaped, through the use of moulds or other means, into almost any desired form with what is often a high degree of durability. This helps in covering a wide measurement range that spreads from the background levels to at least 1 Sv/h of radiation

dose rate. Thin plastic scintillation detectors are also best placed for their utilization in gamma and beta contamination monitors. This is the precise reason why plastic scintillation detectors have found wide applications in the development of radiation portal monitors, contamination monitors and survey meters. Plastic scintillators being of a solid matrix, and when adequately sealed for light and moisture, offer comparable resistance to environmental degradation as that obtained with gas filled radiation detectors. The number of systems based on these detectors is very large over all the segments of the nuclear fuel cycle as well as environmental measurements at all times.

The objective of present work is to provide an impetus to the development of indigenous radiation detectors, Chemistry Division and Radiation Safety System Division, BARC have embarked on a program to initiate the development of organic-inorganic compound-based scintillation radiation detectors and their subsequent incorporation in radiation monitoring systems for deployment in the facilities of DAE.

Gamma survey/dose rate meter

Various compositions were employed using different synthesis techniques to develop a scintillation detector in a cylindrical matrix. Each of the samples generated through the course of this work was characterized for critical parameters such as emission wavelength, intrinsic efficiency, relative scintillation efficiency, transparency and resistance to fading. At least 50 different compositions were synthesized and evaluated. The primary objective of this study was to develop a detector composition with intrinsic efficiency and the scintillation efficiency comparable with that of the commercially procured detectors.

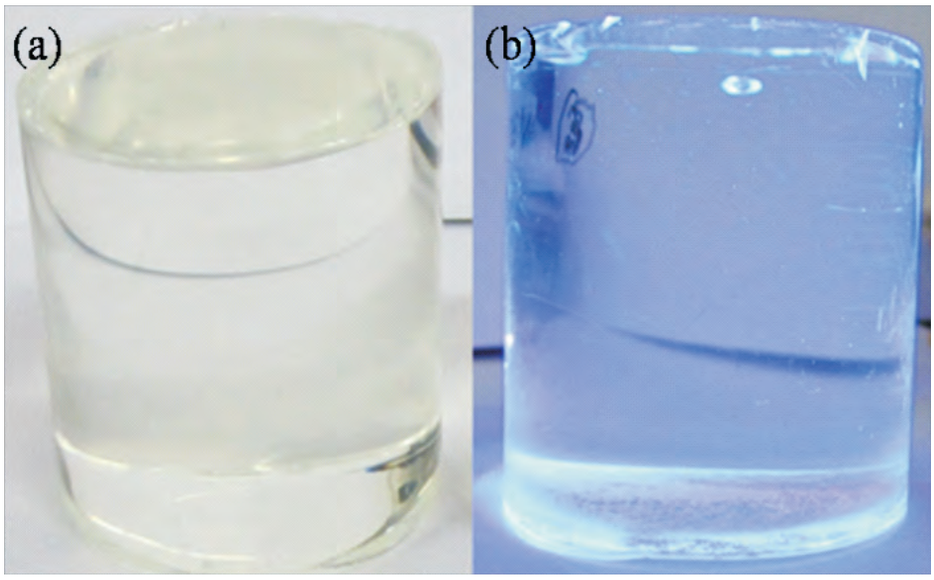

Fig. 1: PVT based plastic detector (5 cm diameter and 5 cm height) developed for survey meter (a) without UV light and (b) with UV light

This was finally realised for a two-dopant system and the characteristics obtained with this system are detailed in the next section. This matrix was subsequently incorporated in to a radiation survey meter, discussed later.

The term "plastic scintillator" typically refers to a scintillating material in which the primary fluorescent emitter, called a fluor, is suspended in the base, a solid polymer matrix of polystyrene (PS) or polyvinyl toluene (PVT), called plastic. The most common type of plastic scintillator is composed of an aromatic plastic base, which has the benzene ring as a pendent group along the polymer backbone. Aromatic structures are necessary for the fluorescence processes of absorption and emission in the area of interest of plastic scintillators. The desired plastic detector for survey meter was accomplished through the dissolution of the primary and secondary fluors in the monomer unit of the base material polyvinyl toluene (PVT) and its subsequent bulk polymerization in a mould of desired shape like cylindrical form. For application in contamination monitors, plastic films have been made by polymerising the ingredients on a 17 cm x 10 cm Perspex block. Figure 1 shows the typical photographs of one of the plastic detectors after synthesis and also after illuminating it with a low power UV LED (390 nm).

Fluorescence occurs in these plastics when energy from ionizing radiation is deposited. The photo-physical properties of a compound are determining factors in its selection for use in a scintillator formulation. The plastic itself, though, is not useful as a scintillator because its fluorescent yield is very low, it is not transparent to its own emission over any appreciable distance (< 1 cm), and its emission spectrum (365 nm) which is in the UV region is too short to match the common photo detectors. The objective of addition of primary and secondary fluors was to make an efficient scintillator by shifting the emission wavelength of polymer to visible range (400-500 nm) besides increasing the bulk attenuation length. These fluors are normally called as wavelength shifters or spectrum shifters. The emission wavelength is shifted from ~365 nm to ~ 400 nm on doping the base plastic PVT with

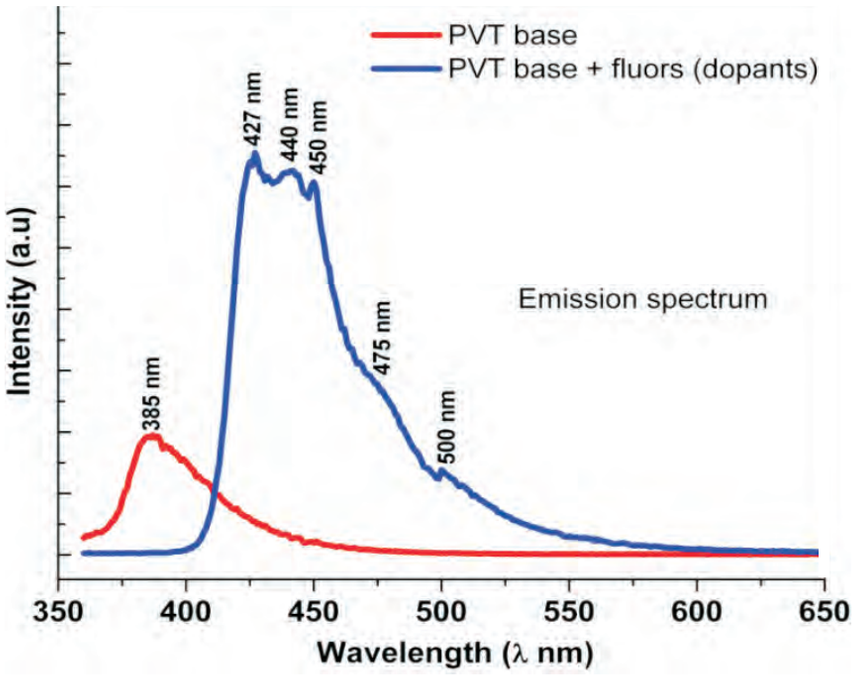

Fig. 2: Emission spectrum of base plastic and plastic detector after excitation at 300 nm

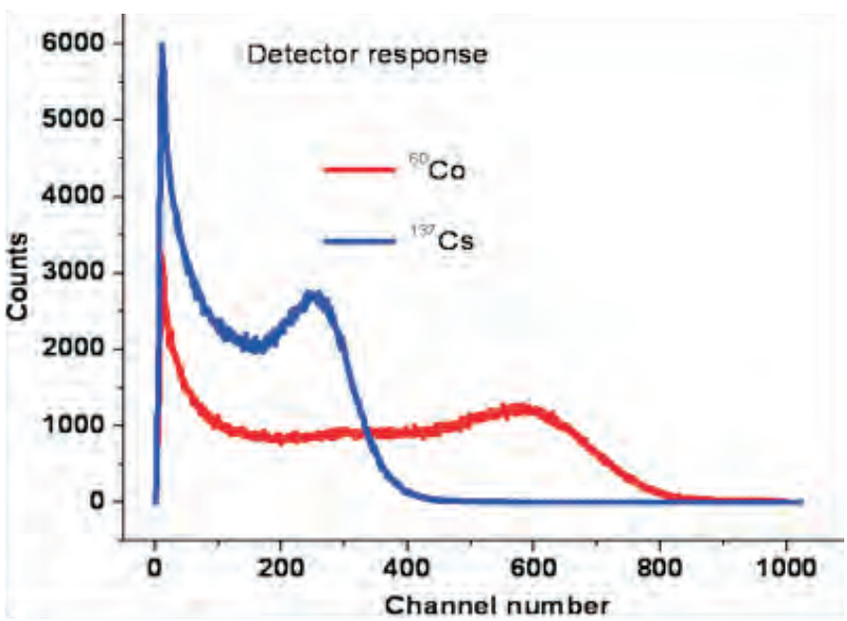

Fig. 3: Detector response to gamma sources ^{137}Cs and ^{60}Co

primary fluor. On further doping the plastic containing primary fluor with the secondary fluor, the emission wavelength shifts from 400 to 410-500 nm, which is in the blue to green range.

Figure 2 shows the emission spectrum on excitation at 300 nm of the base polymer PVT and also the detector obtained after incorporating both the primary and the secondary flours into the plastic base PVT. It is clear from this figure that the final composition emits in the visible light region which is desired for a good plastic detector. It may further be desired to mention that the overlap of the primary fluor absorption spectrum with the emission of the plastic base, as well as overlap of the absorption spectrum of the secondary wavelength shifter with the emission of the primary fluor and subsequent emission in the visible region, is the necessary condition required for the selection of primary and secondary fluors.

The detector matrix, thus generated was evaluated for interaction efficiency and relative light yield with a Photomultiplier unit – amplifier test module coupled to a multi channel analyzer. The output of this configuration processed by PC based software provides the pulse height spectrum. Each sample of detector synthesized during this development phase was evaluated for the pulse height spectra produced as a response to ^{137}Cs and ^{60}Co radionuclide emitted gamma photons and the same was compared with the spectra yielded under identical conditions with commercially available detectors, procured through import (Fig.3). The spread of the spectra provides a measure of the scintillation efficiency. The gross counts recorded in the spectra provide a measure of the interaction efficiency of the detector.

Scintillator detector of diameter 5 cm and height 5 cm was coupled to a photomultiplier tube of compatible spectral response, the output of which was processed with single supply operational amplifier-based amplifier module. The amplifier output was further converted to a CMOS compatible pulse which formed the input to the counting module implemented in a MSP430G2553 microcontroller module. The battery unit comprises of 2 rechargeable batteries of 3.6 V/2.2Ah. An alphanumeric display provides the gamma dose rate measured in terms of Sv/h. The system developed has dimensions of 170 mm x 140 mm x 110 mm weighing 450 gm and the system is shown in Fig. 4.

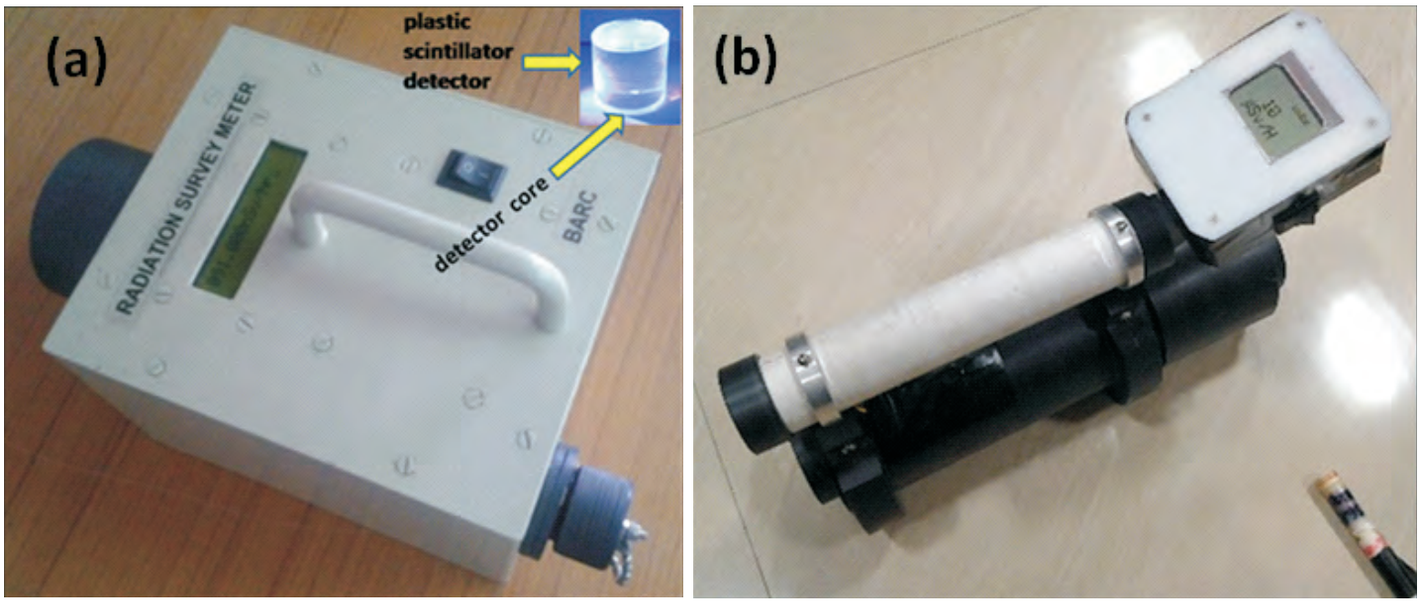

Fig. 4: (a) Gamma survey meter (170 mm x 140 mm x 110 mm) and (b) Dose rate meter, using plastic scintillator

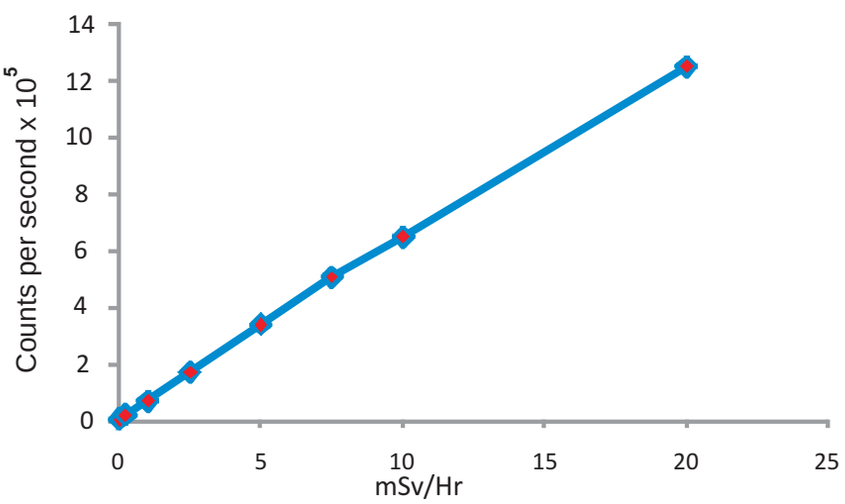

Fig. 5: Dose rate response for the survey meter for ^{137}Cs γ-photons

The system developed as such was calibrated for dose rate response at the Radiation Safety Systems (RSS) facility of Radiation Safety Systems Division (RSSD) with a ^{137}Cs source and the response was found to be approximate a linear fit from 50 nSv/h to 20 mSv/h range. The resulting calibration curve is shown in Fig.5 in terms of cps as a function of dose rate.

The prototype radiation survey meter thus developed has been tested on routine operational basis for monitoring of contaminated material comprising of a large volume of scrap material. The performance of the system has been found to be consistent with that of commercially available survey meters incorporating imported detectors. It did not show any deterioration in performance over a period of 4 years.

Important features of the prototype radiation survey meter are

(a) Efficient radiation dose rate measurement and detection of sources.

(b) Indigenous 2"X2" plastic scintillator detector is employed.

(c) Ultra Low power MSP430G2553 based microcontroller with Nokia 5110 graphical LCD display.

(d) Light weight and portable.

(e) Lithium battery 18650/2200mAh (rechargeable).

Specifications of the meter

(a) Measurement range: Background to 20 mSv/h.

(b) Acquisition time:1sec.

(c) Detector Sensitivity:

3.6 cpm/nSv/h

Beta contamination monitor

The success achieved with the cylindrical matrix provided motivation to explore the possibility to develop a thin film plastic scintillation detector (Fig. 6) for beta measurements. In this case as well after a trial involving many compositions and synthesis protocols the desired results were found for a two-dopant system and a solvent casting method was developed for films. The thin film scintillator thus developed has also been incorporated successfully into a contamination monitor design prototype discussed as follows.

The contamination monitor developed using the thin film plastic scintillation

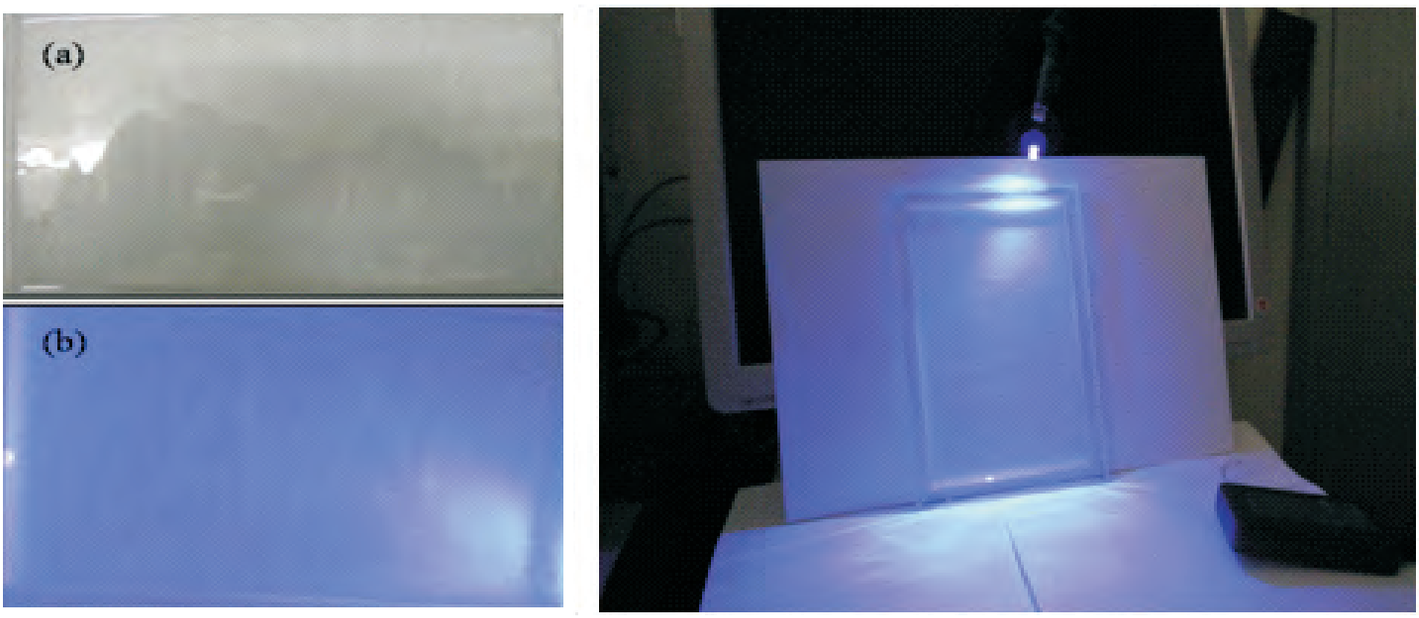

Fig. 6: Thin film plastic scintillators developed for contamination monitor (a) without UV (b) under UV light

Fig. 7: Functional model of thin film scintillator-based contamination monitor

detector has been designed very intricately using a 2ð sensitive PMT housed in a trapezoidal box incorporating a reflective surface.

This design enables the system to have a maximum collection of light at the sensitive area of the PMT. The PMT output is processed further with the help of an amplifier module, the result of which is coupled to a microcontroller module. The active surface area of the system is approximately 170 mm x 100 mm housed in a container with dimensions of 175 mm x 110 mm x 100 mm with a weight approximately equal to 500 g including the display unit.

This system provides a visual display of the radiation interaction with the system in terms of counts per minute. Preliminary studies of the response of the system to a $^{90}Sr/^{90}Y$ source emitted beta particles exposure have provided detection efficiency of the order of approximately 15-20%. Fig. 7 shows the in house assembled contamination monitor made using in-house developed scintillating films.

Important features

(a) Personnel contamination monitoring at nuclear facilities.

(b) Thin plastic scintillator detector with thickness 0.5 mm area 170 cm^2

(c) TFF based PIC24 microcontroller.

(d) Light weight and portable.

(e) 3 Nos. of Li ion batteries (18650).

(f) 20 hours of continuous operation.

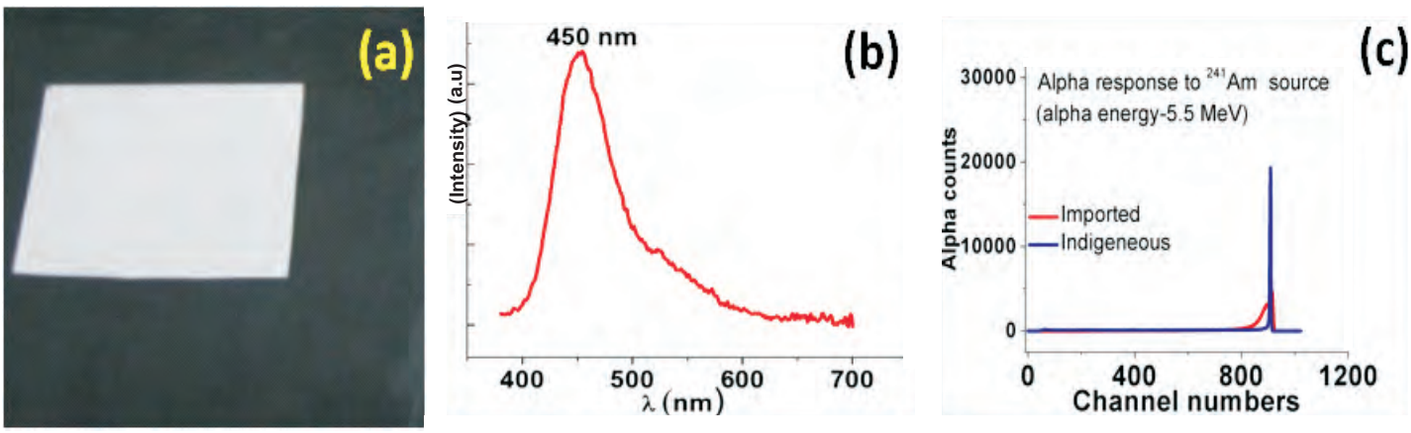

Fig. 8: (a) ZnS:Ag alpha detector, (b) Emission profile of ZnS:Ag excited at 330nm and © comparative response of both imported and indigenous samples of ZnS: Ag to ^{241}Am alpha source

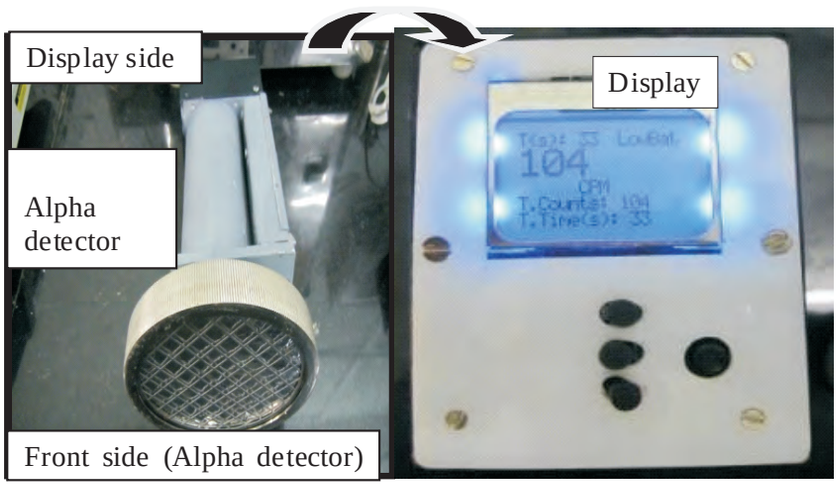

Fig. 9: Alpha detector

Fig. 10: Prototype of indigenously developed alpha and beta contamination monitor

Key specifications

(a) Measurement range: Background to 65000 counts per second (cps).

(b) Acquisition time: 1 sec.

(c) Efficiency for Sr- 90 >18%.

(d) Weight ~500 gm.

Inorganic ZnS: Ag scintillator for alpha particle detector

ZnS:Ag scintillator development has been accomplished during the course of this work. Bulk ZnS powder was mixed thoroughly with required amount of Ag source and heated in an inert atmosphere for 2 h at 900°C and cooled to RT and washed thoroughly. The dried final product is mixed with a binder and screen printed on a transparent surface (Fig. 8a). The photoluminescence of ZnS:Ag (Fig.8b) showed its characteristic blue light emission peak at ~ 450 nm. The testing of this film is carried out in an in-house developed alpha counter system and compared with imported sample. The indigenous ZnS:Ag was comparable with imported system as in Fig. 8c. The indigenous alpha detector system is shown in Figure 9.

Important features

(a) Personnel contamination monitoring at nuclear facilities. Indigenous ZnS(Ag) detector with area approx. 100 cm^2.

(b) Ultra-Low power MSP430G2553 microcontroller.

(c) Light weight and portable.

(d) Four AAC-Zn regular batteries.

(e) 16 h of continuous operation.

Key specifications

(a) Measurement range: Background to 65000 cps.

(b) Acquisition time: 1 min (Auto mode) /User selectable.

(c) Efficiency 25 %. (d) Wt ~500 gm.

Alpha and Beta contamination monitor

Development of a prototype alpha and beta dual purpose contamination monitor by coating ZnS:Ag alpha detector over thin beta detector made using thin film of plastic scintillator is in progress (Fig. 10).

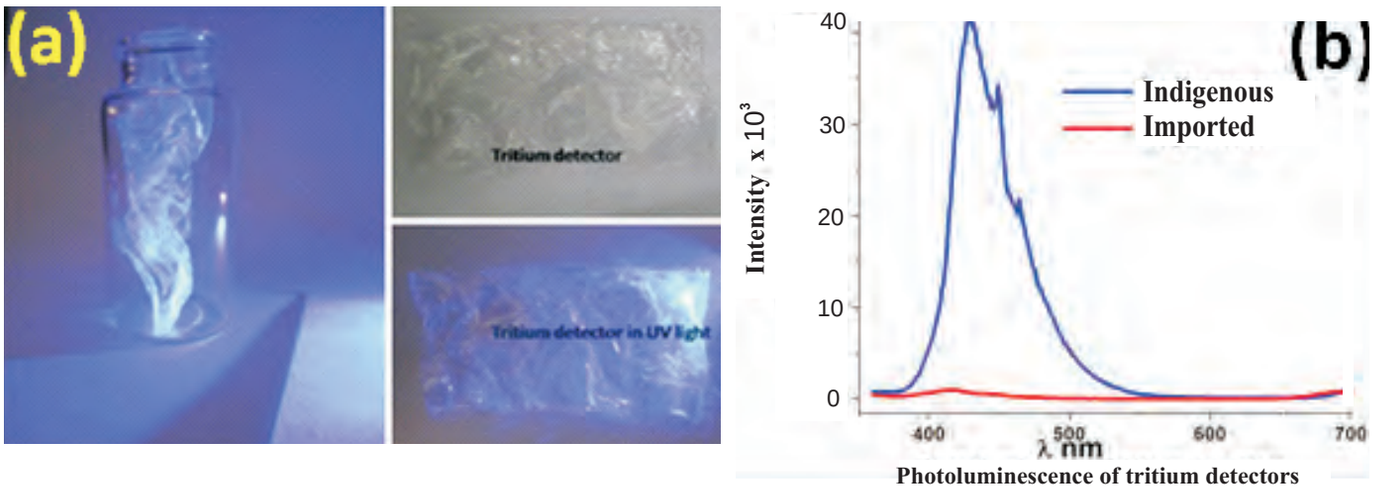

Fig. 11: (a) Image of 10 µm thin film plastic scintillator developed for tritium detection under UV light and (b) photoluminescence of indigenous and imported films

Important features

(a) Prototype of Portable Handheld alpha/Beta/gamma contamination monitoring for nuclear facilities.
(b) Wide area plastic detector / ZnS (Ag) film with area 170 cm^2.
© TFT display based GUI on DSPIC microcontroller platform.
(d) Light weight and highly mobile.
(e) Rechargeable Lithium battery (7.2V).
(f) 20 h of continuous operation.

Key specifications

(a) Combined alpha and beta detection feature.
(b) Acquisition time: 1 sec.
(c) Efficiency for Sr-90(ß) >18 %.
(d) Weight ~1kg.

Development of a new micron thick polymeric scintillator films for tritium detection

Continuous online monitoring of tritium is routinely performed at PHWR facilities in India. Currently µm thick organic scintillator films made from imported NE-102 scintillator is used for monitoring tritium in, (1) air (2) Heavy water and (3) near PHWR plants in DAE. In order to develop in-house developed tritium detector a number of polymers having more number of aromatic structure have been tried and tested. Finally, such a polymer by doping with wavelength shifters is developed and has been tested for tritium (in RSSD) in terms of stability, linearity, sensitivity and efficiency and found to be ~ 15-16 times sensitive and efficient than the imported NE-102 based tritium detector films. Results of photoluminescence plot (Fig 12b) of both samples at RT showed the increased light yield for in-house developed tritium detector.

Conclusion

In-house plastic scintillator-based gamma survey meter and dose rate meter developed and evaluated along with beta contamination monitors. Further import substitute ZnS:Ag alpha detector has been developed and evaluated. A new polymer based thin film scintillator is developed for tritium detection and has shown significantly enhanced response to tritium. The studies demonstrated the capability for development of radiation monitoring systems incorporating in-house developed scintillation detectors that covers a major component of radiation surveillance and safety operations in DAE and also a wide area of operations in the public domain. These studies provide an initial platform to further work towards improvisation and advances in radiation detection and measurement based on scintillation detectors.

***Corresponding author**

Dr. O.D. Jayakumar & Dr. A.K. Tyagi

Acknowledgement

We place on record, our deepest gratitude to Dr. R. M. Suresh Babu, Director, Health, Safety & Environment Group, BARC for his invaluable support, guidance and motivation. We express our most sincere gratitude to Shri V Sathian for his valuable support and counsel in this work. We are indebted to Shri Vishal Kharvi, Smt. Shubangi Wani and Shri D N Patil, RSSD for their endearing efforts in these developmental studies. We are grateful to all our colleagues from RSSD Workshop for their endearing support and contribution in this project.

This page is intentionally left blank

Central Complex BARC

Edited & Published by:
Scientific Information Resource Division
Bhabha Atomic Research Centre, Trombay, Mumbai 400 085, India
BARC Newsletter is also available at URL:http://www.barc.gov.in